NUMERICAL MODELLING OF NON-NEWTONIAN POLARIZABLE AND MAGNETIZABLE FLUID FLOW

Konstantinos Tzirakis[1], Lorenzo Botti[2], Domenico Giordano[3], and Yannis Papaharilaou[1]

[1]*Institute of Applied and Computational Mathematics (IACM), Foundation for Research and Technology-Hellas (FORTH), Heraklion Crete, (Greece), Email: tzirakis@iacm.forth.gr, yannisp@iacm.forth.gr*
[2]*Universtità degli Studi di Bergamo, Engineering Department, 24044 Dalmine (BG), (Italy), Email: bottilorenzo@gmail.com*
[3]*ESA, Aerothermodynamics Section, Nordwijk, (The Netherlands), Email: Domenico.Giordano@esa.int*

ABSTRACT

We extend and validate the pressure correction scheme introduced by Botti and Di Pietro for Newtonian fluids, to non-Newtonian incompressible flows. The scheme consists of a combined set of discontinuous and continuous spaces for velocity and pressure respectively. The varying viscosity is taken into account by adopting the Symmetric Weighted Interior Penalty (SWIP) formulation for the discretization of the viscous stress tensor. We disregard the dependency of the viscosity on spatial derivatives of the velocity in the Jacobian computation, yielding an approximated Jacobian. The convergence rate of the Newton iteration though is not significantly affected, thus preserving the computational efficiency. Numerical accuracy is assessed through analytical test cases, and the method is applied to demonstrate the effects of magnetic fields on fluid flow.

Key words: non-Newtonian fluids; magnetic fields; continuous/discontinuous Galerkin; Symmetric Weighted Interior Penalty (SWIP).

1. INTRODUCTION

Newtonian fluid dynamics have been studied extensively during the past decades. Its relative simplicity was immediately recognized and thus became the standard model in incombressible fluid flows. Soon after it was realized though that many substances deviate from the Newtonian hypothesis. From multiphase systems (like blood) to engineering design solutions, it has been shown that the linear relation between viscosity and shear rate is inaccurate. The transition from the Newtonian to a non-Newtonian consideration is accompanied by a choice for the mathematical model describing it. As a result, many models like the Power-law, Herschel-Bulkley, and Casson [1, 2] amongst others have appeared in the literature.

An interesting feature of many non-Newtonian fluids is their ability to interact with magnetic fields due to the polarizable and magnetizable properties that they possess. As a result, it is possible to alter the flow in such a way in order to enhance or reduce specific flow characteristics. Exploiting magnetic fields thus can have important industrial and clinical applications in industry from magnetic targeted drug delivery to magnetic flow pumps.

The variety of non-Newtonian models requires a tailored solver for numerically simulating such flows efficiently and accurately. To this end, we employ the pressure correction formulation proposed by Botti and Di Pietro [3] for Newtonian flows. In order to account for the varying viscosity we consider the SWIP formulation for the stress tensor, ignoring the dependence of viscosity on the velocity solution in the Jacobian computation. The proposed scheme offers a fast and accurate algorithm for flow simulations of non-Newtonian fluids, where in some cases the computational domain consists of hundreds of thousands if not millions of elements and are characterized by high Reynolds numbers.

2. FLOW MODEL

The Navier-Stokes equations for an incompressible fluid with no temperature dependence are:

$$\nabla \cdot \mathbf{u} = 0, \tag{1a}$$

$$\rho \frac{D\mathbf{u}}{Dt} - \nabla \cdot \boldsymbol{\sigma} = \mathbf{f}, \tag{1b}$$

where $\mathbf{u} \equiv (u, v, w)$ is the velocity vector, ρ and $\mathbf{f}$ are the (constant) density, and body force per unit volume respectively, and $\boldsymbol{\sigma}(\mathbf{u}, p)$ is the stress tensor given by,

$$\boldsymbol{\sigma}(\mathbf{u}, p) = -p\mathbf{I} + \boldsymbol{\tau}(\mathbf{u}). \tag{2}$$

A special class of non-Newtonian fluids (so-called generalized Newtonian) are the ones with shear-stress tensor, $\boldsymbol{\tau}(\mathbf{u})$, of the form,

$$\boldsymbol{\tau}(\mathbf{u}) = 2\eta(\mathbf{D})\mathbf{D} = 2\eta(I_{\mathbf{D}}, II_{\mathbf{D}}, III_{\mathbf{D}})\mathbf{D}, \tag{3}$$

where $\mathbf{D}$ the deformation rate tensor. For incompressible ($I_{\mathbf{D}} = 0$) and shear flows ($III_{\mathbf{D}} = 0$),

$$\boldsymbol{\tau}(\mathbf{u}) = 2\eta(II_{\mathbf{D}})\mathbf{D}. \tag{4}$$

Using finally that the shear rate $\dot{\gamma} \equiv 2\sqrt{II_{\mathbf{D}}}$, we obtain the magnitude of the shear-stress tensor,

$$\tau = \eta(\dot{\gamma})\dot{\gamma}, \tag{5}$$

where in Cartesian coordinates,

$$\begin{aligned}\dot{\gamma}^2 &= 2\left(\frac{\partial u_x}{\partial x}\right)^2 + 2\left(\frac{\partial u_y}{\partial y}\right)^2 + 2\left(\frac{\partial u_z}{\partial z}\right)^2 + \\ &+ \left(\frac{\partial u_x}{\partial y} + \frac{\partial u_y}{\partial x}\right)^2 + \left(\frac{\partial u_x}{\partial z} + \frac{\partial u_w}{\partial x}\right)^2 + \\ &+ \left(\frac{\partial u_y}{\partial z} + \frac{\partial u_w}{\partial y}\right)^2. \end{aligned} \tag{6}$$

A considerable number of generalized Newtonian models have appeared in the literature over the past decades. For the needs of this study though, the Power-law and Herschel-Bulkley models are considered given respectively by,

$$\eta(\dot{\gamma}) = \kappa\dot{\gamma}^{n-1}, \tag{7a}$$

$$\eta(\dot{\gamma}) = (\tau_0/\dot{\gamma})\left[1 - \exp(-m\dot{\gamma})\right] + \kappa\dot{\gamma}^{n-1}, \tag{7b}$$

where κ is the consistency index, n the power index, τ_0 the yield stress, and m the regularization parameter.

In addition, the presence of externally applied magnetic fields may interact with fluids which possess electric and magnetic properties through the coupling between the electromagnetic and flow systems. An induction equation can then be derived which can be coupled to the momentum equations as in the MHD approximation [4]. As a result, a Lorentz force, $\mathbf{J} \times \mathbf{B}$, and a magnetization force, $\mu_0 (\mathbf{M} \cdot \nabla) \mathbf{H}$, are generated yielding the following set of coupled equations,

$$\nabla \cdot \mathbf{u} = 0, \tag{8a}$$

$$\rho\frac{D\mathbf{u}}{Dt} - \nabla \cdot \boldsymbol{\sigma} = \mathbf{J} \times \mathbf{B} + \mu_0 (\mathbf{M} \cdot \nabla) \mathbf{H}, \tag{8b}$$

$$\mathbf{J} = \sigma\mathbf{v} \times \mathbf{B}, \tag{8c}$$

where $\mathbf{B}, \mathbf{H}, \mathbf{M}$, and $\mathbf{J}$ are the magnetic flux density, magnetic field intensity, magnetization, and density of the current respectively. The constant μ_0 is the magnetic permeability of vacuum, and σ is the electric conductivity of the fluid. It should be noted that the electric field is assumed to be negligible and thus does not appear in Ohm's law. In addition, the Lorentz force is not taken into account since we are interested in weak magnetic fields (which can be easily created) characterized by strong spatial gradients.

The applied magnetic field used in this study resembles the one of an ideal dipole which is irrotational[1] and is given by,

$$B_x = -C\left(\frac{2(x - x_i)^2 - r^2}{r^6}\right), \tag{9a}$$

$$B_y = -C\left(\frac{2(x - x_i)(y - y_i)}{r^6}\right), \tag{9b}$$

$$B_z = -C\left(\frac{2(x - x_i)(z - z_i)}{r^6}\right), \tag{9c}$$

where $r = \sqrt{(x - x_i)^2 + (y - y_i)^2 + (z - z_i)^2}$. The field magnitude can then be expressed in terms of the real parameter C as,

$$|B(x, y)| = \frac{C}{r^4}. \tag{10}$$

Using the simplified expression for the magnetization $M = \chi H$ the components of the generated force can be expressed in terms of the constant parameter $\alpha = \mu_0^{-1}\chi/(1 + \chi)^2$ as shown in Tab. 1. Finally, the flows of various models through a straight rigid tube with a 60% axisymmetric stenosis in the presence of the magnetic field of Eq. 9 are also considered. The stenotic geometry is defined by,

$$\mathcal{F}(x) = D/2 - A\mathrm{sech}[\mathrm{B}(\mathrm{x} - \mathrm{x}_0)], \tag{11a}$$

$$y = \mathcal{F}(x)cos\theta, \tag{11b}$$

$$z = \mathcal{F}(x)sin\theta, \tag{11c}$$

where the constants A and B determine the constriction and extension of the stenosis respectively, and x_0 is the x component at the maximum constriction. Concerning the present analysis, the stenosis is parametrized using $A = 0.3D$, $B = 6/D$, $x_0 = 0$, and $D = 0.01$ m. In addition, $(x_i/D, y_i/D, z_i/D) = (0, -0.5, 0)$ and $C = 1.72 \cdot 10^{-10}$ Tm^4, yielding $|B(x, y, z)|_{max} = 4$ T at $(x_0/D, y_0/D, z_0/D) = (\pm 0.2, -0.3, 0)$ as illustrated in Fig. 4.

3. NUMERICAL METHOD

We consider an extension for the incompressible Navier-Stokes solver proposed by Botti and Di Pietro [3] to non-Newtonian fluids. The solver combines a discontinuous Galerkin (dG) approximation for the velocity and a continuous Galerkin (cG) approximation for the pressure, yielding a space couple that is LBB stable for equal order velocity-pressure approximations.

The modification of the solver for generalized Newtonian flows is based on the spatial discretization of the bilinear form of the diffusive term in the momentum equation, $a_h\left(\mathbf{u}_h^{n+1}, \mathbf{v}_h\right)$, for heterogeneous diffusion problems.[2] To this end, two real and non-negative numbers, ω_{T^+} and ω_{T^-}, are assigned for the common face F_f of two elements such that,

$$\omega_{T^+} + \omega_{T^-} = 1, \tag{12}$$

[1] see Tzirakis *et al.* [5] for a detailed analysis of the effect of irrotational forces on fluid flow.

[2] see Ref. [3] for a detailed description of the combined dG-cG scheme devised by Botti and Di Pietro for Newtonian fluids.

Table 1: Components of the magnetization force for an external magnetic field defined by Eqs. 9

coordinate (m)	Magnetization force (N/kg)
x	$f_{Mx} = -\frac{4\alpha C^2}{\rho} \cdot \frac{(x-x_i)^3}{r^{12}}$
y	$f_{My} = -\frac{2\alpha C^2 (y-y_i)}{\rho} \cdot \frac{2(x-x_i)^2+r^2}{r^{12}}$
z	$f_{Mz} = -\frac{2\alpha C^2 (z-z_i)}{\rho} \cdot \frac{2(x-x_i)^2+r^2}{r^{12}}$

where,

$$\omega_{T^-} \equiv \frac{\mu_{T+}}{\mu_{T+} + \mu_{T-}}, \qquad \omega_{T^+} \equiv \frac{\mu_{T-}}{\mu_{T+} + \mu_{T-}}. \quad (13)$$

It is then possible to define a weighted average for the scalar-valued function ϕ as follows,

$$\{\phi\}_\omega \equiv \omega_{T^+}\phi_{T^+} + \omega_{T^-}\phi_{T^-}, \quad (14)$$

with $\{\phi\}_\omega = \phi_T$ at all boundary faces T. It is clear that for homogeneous diffusion problems, definition 14 reduces to the standard arithmetic average. The modification of the diffusive term, $a_h\left(\mathbf{u}_h^{n+1}, \mathbf{v}_h\right)$, using weighted averages was first introduced by Dryja [6] and is usually referred to as the Symmetric Weighted Interior Penalty scheme. It takes the form,

$$\begin{aligned}
&\int_\Omega 2\mu \mathbf{D}_h u_{h,j} : \mathbf{D}_h v_{h,j} + \\
&+ \sum_{F\in\mathcal{F}_h} \frac{\eta\gamma_\mu k^2}{h_F} \int_F [\![\mathbf{u}_h]\!] \cdot [\![\mathbf{v}_h]\!] - \\
&- \sum_{F\in\mathcal{F}_h} \int_F \{2\mu \mathbf{D}_h u_{h,j}\} \cdot \mathbf{n}_F [\![v_{h,j}]\!] - \\
&- \sum_{F\in\mathcal{F}_h} \int_F \{2\mu \mathbf{D}_h v_{h,j}\} \cdot \mathbf{n}_F [\![u_{h,j}]\!], \quad (15)
\end{aligned}$$

where the symbol : denotes the Frobenius inner product, η is a positive penalty parameter independent of the mesh size h and the polynomial degree k, and h_F a local length scale associated with the mesh face. Finally, the diffusion penalty parameter, γ_μ, is defined for all internal faces as [7],

$$\gamma_\mu \equiv \frac{2\mu_{T+}\mu_{T-}}{\mu_{T+} + \mu_{T-}}. \quad (16)$$

4. NUMERICAL VALIDATION

The open source framework `libMesh` [8] is used for the solver implementation. The chosen polynomial spaces are monomials for the discontinuous and Lagrange polynomials for the continuous spaces. Parallelization is performed by `libMesh`, and `PETSc` [9] is chosen for data structures. Mesh partitioning is performed using the `ParMETIS` library [10].

Table 2: Power-law fluid flow between two infinite parallel plates. L^2 errors and corresponding convergence rates of the velocity for a dG(1)-cG(1) scheme.

	velocity	
Mesh	L^2 error $(\times 10^{-3})$	convergence rate
32×32	3.411	
64×64	0.947	1.85
128×128	0.253	1.9
256×256	0.0656	1.95
512×512	0.0166	1.98

Table 3: Power-law fluid flow between two infinite parallel plates. L^2 errors and corresponding convergence rates of pressure for a dG(1)-cG(1) scheme.

	pressure	
Mesh	L^2 error $(\times 10^{-3})$	convergence rate
32×32	3.852	
64×64	1.032	1.9
128×128	0.267	1.95
256×256	0.068	1.97
512×512	0.0174	1.98

The temporal accuracy of the scheme is not examined since it has been confirmed for the Newtonian case in [3]. In order to numerically assess the spatial convergence rates, the flow of a power-law fluid between two infinite parallel plates is considered in the two-dimensional domain $(0, 10) \times (-1, 1)$. The discretization scheme is an equal order dG(1)-cG(1). The simulation is performed at $Re = 80$, and weakly Dirichlet boundary is enforced to the exact solution. The initial conditions on the computational domain are set to zero velocity and pressure. In order to obtain a steady solution, a time integration is performed assuming a fixed step $\Delta t = 0.1$ s. The L^2 errors for both the velocity and pressure are shown in Tabs. 2 and 3 respectively.

The theoretical convergence rates of h^{k+1} for the L^2 error on the velocity is confirmed for the dG(1)-cG(1) discretization. The convergence rates for the pressure are

Table 4: Percentage RMS errors with respect to u_{mean} for different values of n.

n	% RMS error w.r.t. u_{mean}
$3/6$	$5.8 \cdot 10^{-3}$
$4/6$	$5.6 \cdot 10^{-3}$
$5/6$	$4.8 \cdot 10^{-3}$

higher than expected due to the linear nature of the pressure exact solution, while first order convergence is expected in general for a dG(1)-cG(1) discretization.

5. TEST CASE: COUETTE FLOW

The Couette flow of a power-law model is studied as a validation case for the solver. The channel's width is $L = 0.01$ m and its length $l = 0.5$ m. Three different values of the exponent are considered ($n = 3/6, 4/6, 5/6$), whereas the consistency index is kept constant and equal to $0.0035\ \mathrm{Pa} \cdot \mathrm{s^n}$. The simulations run at $Re = 100$, $\Delta t = 2 \cdot 10^{-3}$ s, and the fully developed Newtonian velocity profile is prescribed at the inlet. The numerical results are then compared to the analytical solution for Couette flow of a power-law fluid,

$$\frac{u}{u_{mean}} = \frac{2n+1}{n+1}\left[1 - \left(\frac{y}{H}\right)^{1/n+1}\right], \qquad (17)$$

where y denotes the distance in the transverse direction from the centerline, and $H = L/2$.

RESULTS: The percentage RMS error divided by u_{mean} at $x/L = 50$ is shown in Tab. 4 where it can easily be seen that is practically negligible for all cases. Fig. 1 presents the non-dimensional velocity, $u/u_{max,n}$, where $u_{max,n}$ is the maximum velocity along the centerline for each power-law model. Simulations initiate from a different $u/u_{max,n}$ ratio, but they all converge to unity as each one reaches the corresponding maximum velocity for the specific choice of parameters. Obviously, the length required for convergence is inversely related to the value of the exponent thus requiring more channel lengths for smaller values of n. Fig. 2 shows the non-dimensional velocity ratio $u/u_{max,n}$ at $x/L = 50$. Again, all simulations have a maximum value of unity at $y/H = 0$ independent of the specific model. Finally, Fig. 3 shows the velocity profiles for the three cases considered at $x/L = 0$, $x/L = 10$, and $x/L = 20$, where it can easily be seen that all cases start from the imposed Newtonian profile at the inflow, but they later split according to the assumed parameteres.

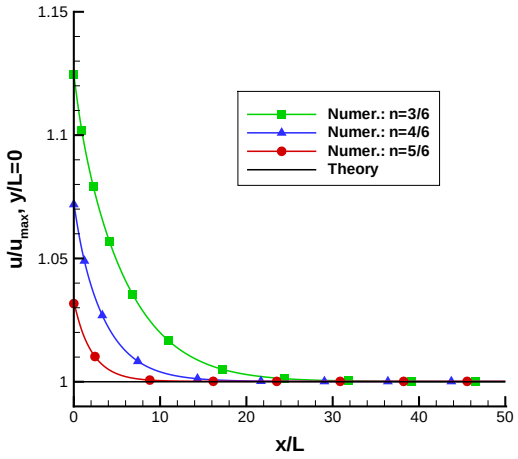

Figure 1: Couette flow: non-dimensional velocity of a power-law fluid for different values of exponent n at $y/L = 0$.

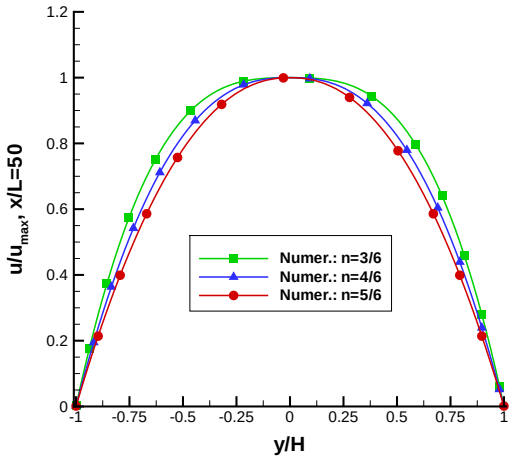

Figure 2: Couette flow: non-dimensional velocity profiles of a power-law fluid for different values of exponent n at $x/L = 50$.

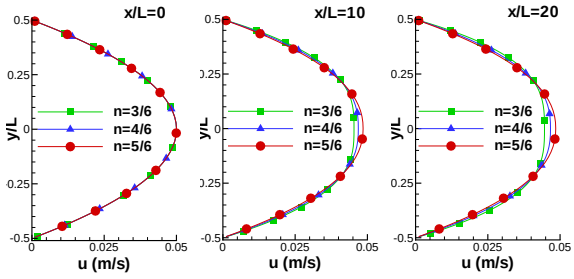

Figure 3: Couette flow: splitting of the velocity profiles in terms of the parameters for a power-law fluid.

6. APPLICATION: STENOSIS FLOW

The steady flow of a Newtonian and a Herschel-Bulkley fluid through the stenosis is presented in this section. The simulations run at $Re = 100$ and $\Delta t = 5 \cdot 10^{-3}$ s. The fully developed parabolic profile is prescribed again at the inlet. The following set of parameters is taken for the Herschel-Bulkley fluid [11]: $\tau_0 = 0.0035$ Pa, $n = 0.8375$, $\kappa = 0.008\ \mathrm{Pa} \cdot \mathrm{s}^{0.8375}$, $m = 1000$ s, and $\chi = 3.5 \cdot 10^{-6}$.

RESULTS: Fig. 5 presents the centerline velocity of both fluids and their interaction with the externally applied magnetic field of Eqs. 9. Due to the shear-thinning effect, the flattened profile of the Herschel-Bulkley model yields a smaller maximum velocity. The addition of the magnetic field pushes both fluids towards the wall, reducing the streamwise component along the axis of symmetry. In both cases though, the effect of the magnetic field diminishes approximately nine diameters in the post-stenotic region. Finally, from Fig. 6 it can easily be seen that even a moderate magnetic field which is characterized by strong spatial gradients can alter the flow of a magnetizable fluid.

7. CONCLUSIONS

A pressure-correction scheme for the flow of non-Newtonian and incompressible fluids is presented. The scheme consists of a combined discontinuous Galerkin approximation for the velocity, and a standard continuous Galerkin approximation for the pressure. The stress-tensor is not discretized separately but rather is computed explicitly thus disregarding its non-linearity in the Jacobian computation. We also demonstrate the ability of the method to accurately resolve multidimensional benchmark problems. The method is subsequently utilized to assess the effects of magnetic fields on fluid flow, and can potentially have important industrial applications such as the development of magnetic pumps.

ACKNOWLEDGMENTS

This work has been supported by the ESA TRP program.

REFERENCES

[1] Sankara D.S., Lee U., 2009, Communications in Nonlinear Science and Numerical Simulation 14, 2971

[2] Chaturani P., Ponnalagar Samy R., 1986, Biorheology 23, 499

[3] Botti L., Di Pietro D.A., 2011, J. Comput. Physics 230, 572

[4] Pai, SI., 1955, Magnetohydrodynamics and Magnetogasdynamics, PN

[5] Tzirakis K., Papaharilaou Y., Giordano D., Ekaterinaris J., 2013, Int J Numer Method Biomed Eng 30, 297

[6] Dryja M., 2003, Comput. Methods Appl Math 3, 76

[7] Di Pietro D.A., Ern A., Guermond J.L., 2008, SIAM J Numer Anal 46, 805

[8] Kirk B.S., Peterson J.W., Stogner R.H., et al., 2006, Eng Comput 22, 237

[9] Balay S., Abhyankar S., Adams M., et al., 2014, Argonne National Laboratory

[10] Karypis G., Kumar V., 1999, SIAM Journal on Scientific Computing 20, 359

[11] Valant A.Z., Žiberna L., Papaharilaou Y., Anayiotos A., Georgiou G., 2011, Rheologica Acta 50, 389

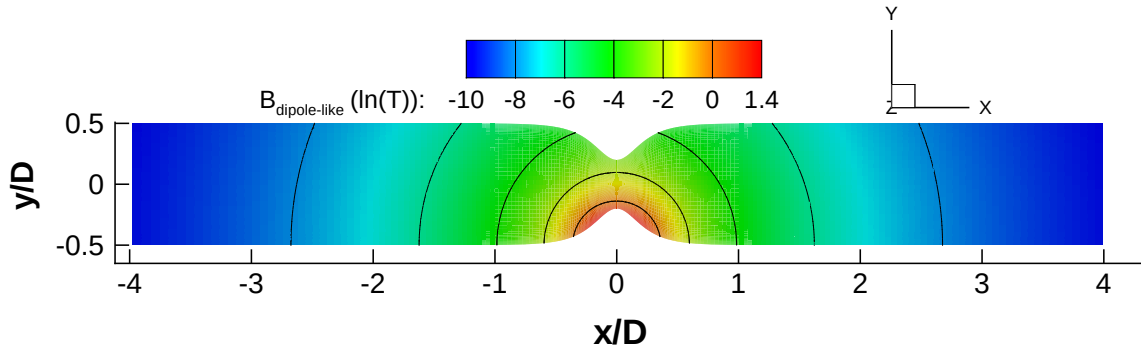

Figure 4: Magnitude contours of the external magnetic field given by Eqs. 9. The intensity of the field is plotted on a natural logarithmic scale.

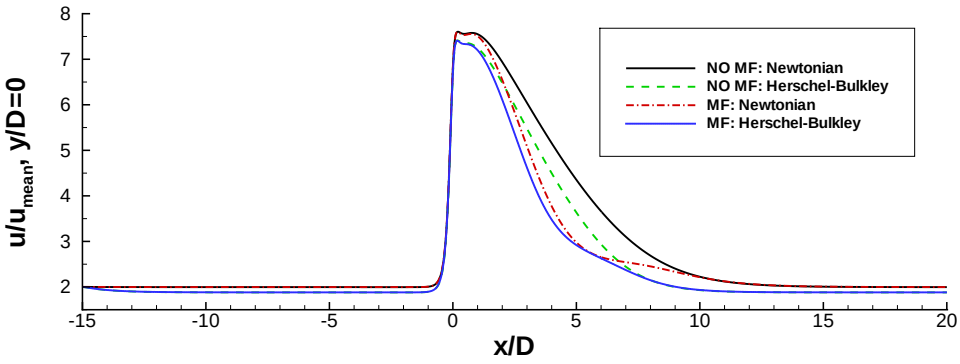

Figure 5: Non-dimensional centerline velocity in the absence of external magnetic fields for a Newtonian (black solid) and Herschel-Bulkley (green dashed) fluids, and when the field of Eqs. 9 is turned on for the Newtonian (red dashed-dotted) and Herschel-Bulkley (blue dotted) fluids. In all cases, the Newtonian velocity profile is prescribed at the inlet.

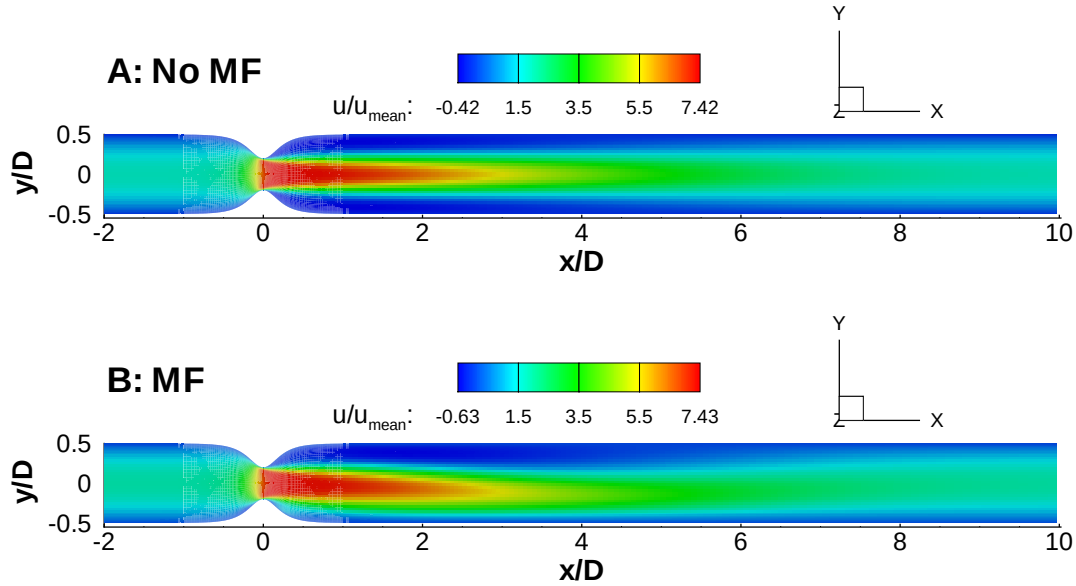

Figure 6: Non-dimensional velocity of a Herschel-Bulkley fluid for two cases. A: in the absence of external magnetic fields and B: when the magnetic fields is turned on. The generated magnetization force pushes the flow towards the lower wall.